Evolutionary plasticity in the allosteric regulator-binding site of pyruvate kinase isoform PykA from *Pseudomonas aeruginosa*

Received for publication, May 2, 2019, and in revised form, August 21, 2019 Published, Papers in Press, September 4, 2019, DOI 10.1074/jbc.RA119.009156

Yassmin Abdelhamid[‡], Paul Brear[‡], Jack Greenhalgh[§], Xavier Chee[§], Taufiq Rahman[§], and Martin Welch[‡1]

From the [‡]Department of Biochemistry, University of Cambridge, Cambridge CB2 1QW, United Kingdom and the [§]Department of Pharmacology, University of Cambridge, Cambridge CB2 1PD, United Kingdom

Edited by Ruma Banerjee

Unlike many other well-characterized bacteria, the opportunistic human pathogen *Pseudomonas aeruginosa* relies exclusively on the Entner-Doudoroff pathway (EDP) for glycolysis. Pyruvate kinase (PK) is the main "pacemaker" of the EDP, and its activity is also relevant for *P. aeruginosa* virulence. Two distinct isozymes of bacterial PK have been recognized, PykA and PykF. Here, using growth and expression analyses of relevant PK mutants, we show that PykA is the dominant isoform in *P. aeruginosa*. Enzyme kinetics assays revealed that PykA displays potent K-type allosteric activation by glucose 6-phosphate and by intermediates from the pentose phosphate pathway. Unexpectedly, the X-ray structure of PykA at 2.4 Å resolution revealed that glucose 6-phosphate binds in a pocket that is distinct from the binding site reported for this metabolite in the PK from *Mycobacterium tuberculosis* (the only other available bacterial PK structure containing bound glucose 6-phosphate). We propose a mechanism by which glucose 6-phosphate binding at the allosteric site communicates with the PykA active site. Taken together, our findings indicate remarkable evolutionary plasticity in the mechanism(s) by which PK senses and responds to allosteric signals.

Pyruvate kinase (EC 2.7.1.40) is a key enzyme in glycolysis, and a major site of pathway regulation. The enzyme catalyzes the conversion of phospho*enol*pyruvate and ADP into pyruvate and ATP (1). Given its central position in metabolism, pyruvate kinase (PK)[2] activity can have a major impact on the carbon economy of the cell (2, 3). More recently, it has been shown that PK activity can also influence pathogencity (4). Bacterial PK is encoded by two isozymes, *pykA* and *pykF* (5–7). Most organisms encode either *pykA* or *pykF*, although a few species also encode both isozymes. Among the organisms encoding both *pykA* and *pykF* that have been characterized to date, PykF is usually the dominant isoform. The PykA and PykF isozymes have been especially well-studied in the *Enterobacteriaceae*, and are distinguished by being differentially regulated and cladistically distinct (at a sequence level). For example, PykF isozymes are typically activated by fructose 1,6-bisphosphate (8), whereas PykA is activated by adenosine 5′-monophosphate (AMP) (9). Several crystal structures are available for PykF isozymes, although no structures have been solved for PykA. Recently, the structure of *Mycobacterium tuberculosis* PK bound to AMP and glucose 6-phosphate was solved (the first structure to be solved for a bacterial PK with bound allosteric regulators). The regulators were found to bind at distinct sites in the allosteric cleft and were proposed to communicate with the active site through a series of domain re-orientations denoted the "rock-shape-lock" mechanism.

Pseudomonas aeruginosa is an opportunistic pathogen that commonly causes pulmonary (10), urinary tract (11), and soft tissue-associated infections in hospitalized patients. The pathogen is intrinsically resistant to most clinically-used antibiotics (12) and was recently designated by the World Health Organization (WHO) as a "critical priority pathogen." Unlike the *Enterobacteriaceae*, which mainly employ the Embden-Meyerhof-Parnas (EMP) pathway for glucose catabolism, *P. aeruginosa* lacks phosphofructokinase and utilizes the Entner-Doudoroff pathway (EDP) instead (13, 14). As a consequence, PK is likely to be the major site of glycolytic flux regulation in this organism. *P. aeruginosa* encodes two uncharacterized PK isozymes, annotated as *pykA* (PA4329) and *pykF* (PA1498). Here, we show that in contrast with most organisms encoding both PK isozymes, in *P. aeruginosa*, PykA plays the dominant physiological role. We also present the first structure of a PykA isozyme. Surprisingly, this structure revealed that glucose 6-phosphate binds in a site distinct to that observed for the *M. tuberculosis* enzyme.

Results

PykA is the dominant pyruvate kinase isozyme in P. aeruginosa

P. aeruginosa encodes two PK isozymes: PykA (PA4329, 58% amino acid identity with *Escherichia coli* PykA) and PykF (PA1498, 37% amino acid identity with *E. coli* PykF). An alignment of selected relevant PykA and PykF sequences is shown in

This work was supported by a Ph.D. studentship from the Yousef Jameel Foundation (to Y. A.), a BBSRC studentship (to J. G.), and BBSRC Grant BB/M019411/1. The authors declare that they have no conflicts of interest with the contents of this article.

This article contains Figs. S1–S13 and Table S1.

The atomic coordinates and structure factors (code 6QXL) have been deposited in the Protein Data Bank (http://wwpdb.org/).

[1] To whom correspondence should be addressed. Tel.: 0044-0-1223-333-653; E-mail: mw240@cam.ac.uk.

[2] The abbreviations used are: PK, pyruvate kinase; KDPG, 2-*keto*-3-deoxy-6-phosphogluconate; EDP, Entner-Doudoroff pathway; PEP, phospho*enol*-pyruvate; F6P, fructose 6-phosphate; G6P, glucose 6-phosphate; R5P, ribose 5-phosphate; RL5P, ribulose 5-phosphate; X5P, xylulose 5-phosphate; LDH, lactate dehydrogenase; BIS-TRIS propane, 1,3-bis[tris(hydroxymethyl)methylamino]propane; PDB, Protein Data Bank; RMS, root mean square; G3P, glyceraldehyde 3-phosphate.

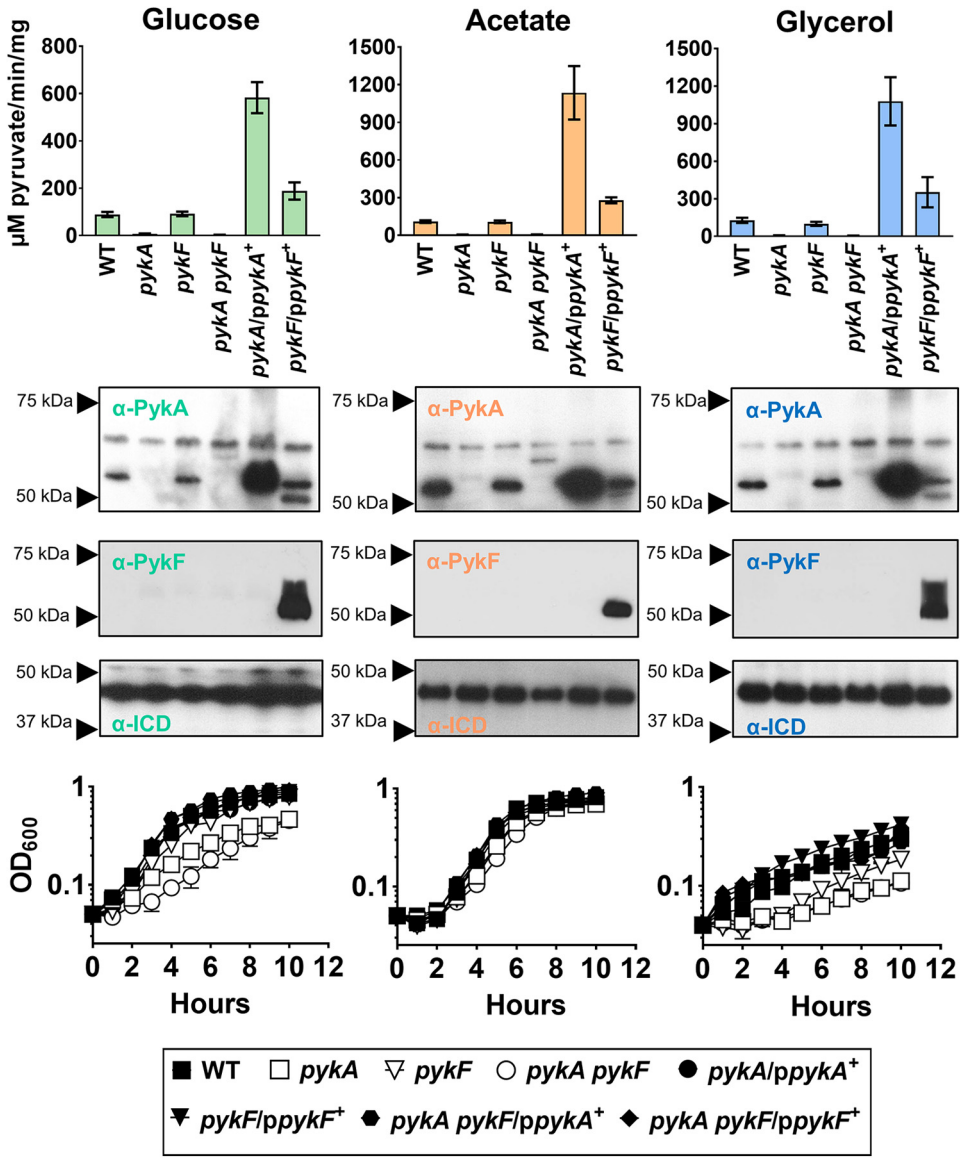

Figure 1. PykA is the dominant PK in *P. aeruginosa*. *Upper panel*, PK activity of the WT and indicated mutants grown in M9 minimal media supplemented with 20 mM glucose, 30 mM glycerol, or 40 mM acetate. Where indicated, the *pykA* mutant, *pykF* mutant, or *pykA pykF* double mutant were complemented with a plasmid expressing *pykA* (denoted p*pykA*$^+$) or *pykF* (denoted p*pykF*$^+$). Cell cultures were collected for measurement of enzyme activity after 10 h of growth. *Middle panel*, Western blots showing expression of PykA and PykF (as indicated) in the different carbon sources. Isocitrate dehydrogenase (*ICD*) was probed using anti-ICD antibodies as a loading control in each blot. The doublet observed when anti-PykA antibodies were used to probe cell extracts of the *pykF* mutant expressing *pykF* in *trans* indicates weak cross-reactivity of the anti-PykA antibodies with PykF (the lower of the bands in the doublet being PykF). No such cross-reactivity was apparent with the anti-PykF antibodies. *Lower panel,* growth of the indicated PK mutants (± complementation) in different carbon sources. Data represent mean ± S.D. for three independent biological replicates.

Fig. S1. Phylogenetic classification of *P. aeruginosa* PykA and PykF (Fig. S2) indicates that the isozymes belong to two distinct subclasses of PK. To establish which isozyme is dominant in *P. aeruginosa*, we measured the PK activity in cell extracts of mutants defective in *pykA*, *pykF*, or *pykA* and *pykF* together (*pykA pykF*). Following growth on minimal medium containing glucose, glycerol, or acetate as a sole carbon source, pyruvate kinase activity was >90% lower in the *pykA* mutant and in the *pykA pykF* mutant than it was in the WT control (Fig. 1). However, pyruvate kinase activity in the *pykF* mutant remained high on these substrates. These data indicate that PykA contributes most to PK activity in *P. aeruginosa*. Consistent with this, Western analyses using antibodies raised against purified *P. aeruginosa* PykA or PykF confirmed that the latter is essentially undetectable during growth on the carbon sources tested unless overexpressed in *trans* from a plasmid (Fig. 1). Note that the antibodies were preabsorbed against a *pykA* mutant (for the anti-PykA antibodies) or a *pykF* mutant (for the PykF antibodies). The absence of PykF expression in a *pykA* mutant led to weak cross-reactivity of the anti-PykA antibodies against shared PykA/PykF epitopes in PykF, although this was only apparent when PykF was overexpressed. We conclude that *pykA* is expressed at higher levels in these conditions than *pykF*.

To explore the phenotypic consequences of *pykA* and *pykF* mutation, we assessed the growth characteristics of each mutant on different carbon sources (Fig. 1). The *pykA* mutant and the *pykA pykF* mutant grew slowly compared with the WT and the *pykF* mutant in minimal media containing glucose or

glycerol as a sole carbon source. That there was any observable growth of these mutants at all on glucose is presumably due to the pyruvate produced at the 2-*keto*-3-deoxy-6-phosphogluconate (KDPG) aldolase-catalyzed step of the EDP. Similarly, the slow, but nonnegligible growth in glycerol (which feeds in to the EDP after the KDPG aldolase-catalyzed step) can be rationalized by invoking operation of the recently-defined EDEMP cycle (15). The EDEMP cycle allows triose phosphates such as those derived from glycerol to be recycled through the KDPG aldolase step, thereby yielding pyruvate. Growth on glucose or glycerol was restored in the *pykA* mutant and the *pykA pykF* mutant by expression of either *pykA* or *pykF* in *trans*, suggesting that both isozymes have the potential to complement the *pykA* mutant growth defect. These data also indicate that the low PK activity in the *pykA* mutant is likely due to low expression of PykF, rather than low intrinsic activity of the isozyme. Consistent with this, pyruvate kinase activity increased and PykF expression became detectable during growth on glucose when *pykF* was expressed in *trans* in the *pykF* mutant (Fig. 1). (*PykF* is predicted to be part of a bicistronic operon alongside a putative glycerate kinase, PA1499. The p*pykF*$^+$ complementation plasmid encoded both PA1499 and *pykF*, see "Materials and Methods".) In contrast, during growth on acetate, the *pykA*, *pykF*, and *pykA pykF* mutants all grew at essentially the same rate as the WT. This suggests that PykA plays an important role in catabolizing substrates that feed into the EDP such as glucose and glycerol, but contributes less to growth on acetate (which does not require flux through the PK-catalyzed reaction).

Kinetic properties and regulation of PykA

Purified PykA was an ~200 kDa tetramer in solution based on analytical ultracentrifugation data (Figs. S5 and S6). At saturating phospho*enol*pyruvate (PEP) concentration, the enzyme displayed Michaelis-Menten kinetics with respect to [ADP], with a K_m value of 0.07 mM (Fig. 2, Table 1). In contrast, at saturating ADP concentration, the PEP-dependence was sigmoidal, with an $s_{0.5}$ value of 0.67 mM (Fig. 2, Table 1) and a Hill coefficient of 2.14, indicative of positive cooperativity.

All PK enzymes require divalent cations for activity (mostly Mg^{2+}), and some have also been reported to require K^+ to achieve maximum catalysis (16). The presence of these ions is important to facilitate binding of the substrate, transfer of the phosphoryl group from PEP to ADP, and possibly also acquisition of an active enzyme conformation (17, 18). We found that the activity of *P. aeruginosa* PykA was independent of K^+ concentration (Fig. 2). Indeed, addition of monovalent cations (K^+, NH_4^+ or Na^+) even somewhat decreased the overall catalytic activity of the enzyme (Fig. S7, Table 1). The K^+-mediated activation of pyruvate kinase activity is known to be dependent on the nature of the residue immediately preceding strand Bβ1 in the structure (19); in K^+-dependent enzymes, this residue is a glutamate, whereas in K^+-independent enzymes, it is often a lysine. In *P. aeruginosa* PykA, the corresponding residue is a lysine (Fig. S1).

Pyruvate kinase is a major site for the regulation of glycolytic flux in many species, and most of the known regulators in other species are associated with the EMP. However, *P. aeruginosa* relies solely on the EDP for glycolysis. To investigate the regulation of *P. aeruginosa* PykA further, we screened a wide range of metabolic intermediates, guided by a knowledge of the pathways feeding in and out of the EDP, for their ability to activate or inhibit PykA *in vitro*. Putative regulatory molecules were screened at low PEP concentration (0.3 mM) to identify activating ligands, and high PEP concentration (3 mM) to identify inhibitory ligands (Fig. 2 and Fig. S8, respectively). More detailed kinetic analyses ($s_{0.5}$, k_{cat}) were carried out on the "hits" identified this way (Fig. 2, Fig. S9, and Table 1). No inhibitors were identified. However, PykA was strongly activated by glucose 6-phosphate (G6P) from the EDP and by intermediates from the reductive PPP (fructose 6-phosphate (F6P), glyceraldehyde 3-phosphate (G3P), ribose 5-phosphate (R5P), ribulose 5-phosphate (RL5P), and xylulose 5-phosphate (X5P)) (Table 1). The main effect of these regulators was to decrease $s_{0.5}$, suggestive of K-type allosteric regulation, and to change the substrate dependence kinetics on PEP from a sigmoidal to a hyperbolic (*i.e.* Michaelis-Menten) profile. Although these regulators had a large impact on the PEP-dependence of the reaction, they had little or no effect on its ADP-dependence. Interestingly, AMP and fructose 1,6-bisphosphate (two well-established regulators of PK in many other species) had almost no effect on PykA activity.

Structure of PykA

Currently, there is no structure available for any PykA isozyme. We were therefore fortunate to obtain crystals of PykA containing a substrate analogue (malonate) and Mg^{2+} bound in the active site, and a bound allosteric regulator (G6P). The crystals diffracted X-rays to 2.4 Å resolution. The asymmetric unit of PykA contained 12 polypeptides assembled into three complete homotetramers. This quaternary structure is consistent with analytical ultracentrifugation analyses data indicating that PykA is a tetramer in solution (Fig. S6). Refinement statistics are shown in Table 2.

Each protomer of PykA had the typical tripartite domain organization associated with PKs, with the A and C domains of one protomer interacting with the A and C domains, respectively, from the adjacent protomers (Fig. 3, *A* and *B*). The A domain is comprised of 8 α/β structures assembled into a TIM barrel motif. Helices Aα6 and Aα8 are further subdivided into shorter segments forming Aα6′ and Aα8′. The Aα6′helix contains part of a highly conserved segment (^{245}MVARGDLGVE^{254}), which plays a key role in catalysis (Fig. 3*C*). The active site is located in the cleft between domains A and B (Fig. 3*B*). Relative to the A domain, the spatial disposition of the β-rich B domain varied somewhat between the different protomers, indicating that the domain is configurationally flexible as a unit. The $\alpha\beta$-rich C domain contains the bound allosteric regulator, G6P.

The PykA active site contains a bound substrate analogue, malonate (present in the crystallization buffer), and Mg^{2+} (Fig. 3*C*). The malonate is bound by hydrogen bonds from both the polypeptide backbone (residues Gly^{249} (2.8 Å) and Asp^{250} (3.1 Å)) and the side chains of Lys^{221} (2.9 Å), Thr^{282} (2.6 Å), and Arg^{34} (3.3 Å). In addition, the active site Mg^{2+} also contributes to malonate binding through electrostatic interactions. The Mg^{2+} is octahedrally coordinated through interactions with

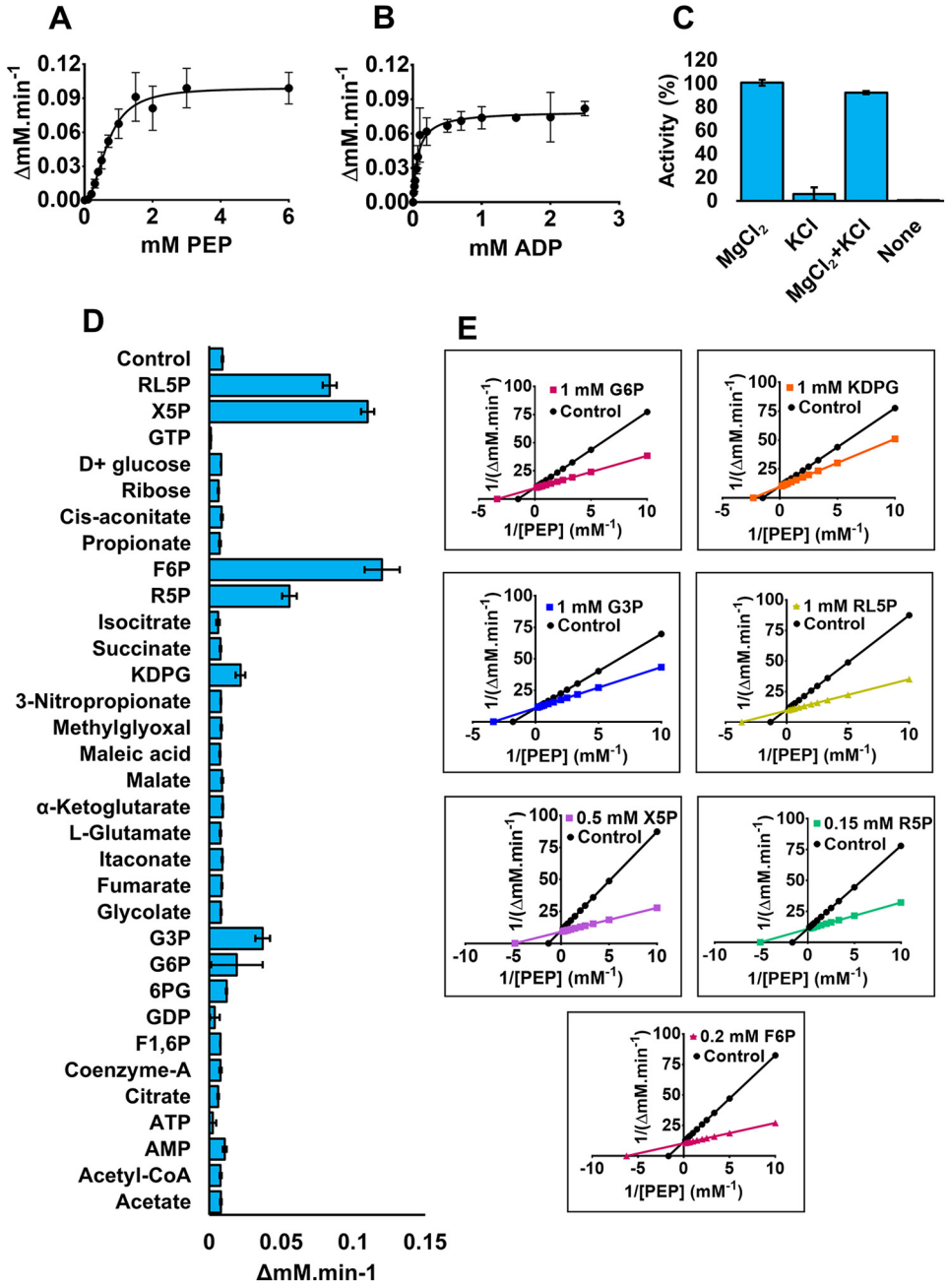

Figure 2. Kinetic characterization of PykA. *A* and *B,* PykA kinetics with respect to PEP and ADP. The PEP titration was carried out using a saturating concentration of ADP (2 mM), whereas the ADP titration was carried out using a saturating concentration of PEP (5 mM). *C,* effects of monovalent and divalent cations on PykA activity. $MgCl_2$ and KCl were added at 10 and 100 mM concentrations, respectively. PEP and ADP were at saturating initial concentrations (5 and 2 mM, respectively). *D,* the effect of putative metabolic regulators on PykA activity at low [PEP] (0.3 mM). [ADP] was fixed at 2 mM. The rationale here was to identify potential activatory molecules. Potential regulators were added at a final concentration of 1 mM, except for F6P, R5P, and X5P, which were added at 0.2, 0.15, and 0.5 mM concentration, respectively. Data of *A–D* represent the mean ± S.D. of three independent experiments. *E,* Lineweaver-Burk plots demonstrating that the indicated metabolic molecules primarily act to decrease $s_{0.5}$ of PykA compared with control (without regulators).

the side chains of Glu^{223} and Asp^{250}, and also with two water molecules. These active site residues are absolutely conserved in all bacterial PKs (Fig. S1), as is their spatial disposition, even when comparing malonate-bound PykA with pyruvate-bound PK from rabbit muscle (PDB 1F3W) (Fig. 3*D*). In contrast, superposition of the PykA active site with that of *E. coli* apo-PykF (PDB 1PKY) reveals that almost all the residues just discussed undergo significant spatial re-orientation in the presence of the substrate, indicative of induced fit (Fig. 3*E*).

An alignment of PykA sequences reveals that all PykA orthologues contain 3 residues not present in any of the PykF orthologues, corresponding to Ala^{229}, Asp^{230}, and Asp^{231} in *P. aeruginosa* PykA (Fig. S1). The presence of these three additional residues lengthens the loop connecting Aα5-Aβ5 resulting in the displacement of helix Aα5 away from the core of the enzyme (Fig. S10). The functional significance of this is not yet clear, although it is worth noting that the same loop of structure contributes two key residues to the active site: Glu^{223} and Lys^{221} (Fig. S10).

Table 1
The effect of metabolic regulators and monovalent ions on PykA activity
Kinetic parameters were calculated using GraphPad Prism from best-fit nonlinear regression analysis of the data. The allosteric sigmoid function was used for the PEP titration and the Michaelis-Menten function was used for ADP titration.

	No additive	0.2 mM F6P	0.15 mM R5P	1 mM G3P	1 mM G6P	1 mM KDPG	0.5 mM X5P	1 mM RL5P	100 mM KCl	100 mM NH_4Cl	100 mM NaCl
PEP titration											
$s_{0.5}$ (mM)	0.670 ± 0.058	0.159 ± 0.021	0.195 ± 0.017	0.297 ± 0.017	0.290 ± 0.026	0.432 ± 0.036	0.209 ± 0.011	0.269 ± 0.012	1.187 ± 0.086	1.402 ± 0.084	1.492 ± 0.116
Hill coefficient (*h*)	2.14 ± 0.34	1.45 ± 0.31	1.65 ± 0.25	1.89 ± 0.21	1.78 ± 0.32	1.52 ± 0.18	1.87 ± 0.22	1.61 ± 0.12	2.36 ± 0.28	2.31 ± 0.22	2.42 ± 0.32
V_{max} (mM/min)	0.099 ± 0.004	0.096 ± 0.004	0.092 ± 0.003	0.092 ± 0.002	0.100 ± 0.003	0.100 ± 0.004	0.110 ± 0.002	0.110 ± 0.002	0.087 ± 0.002	0.130 ± 0.003	0.120 ± 0.004
$k_{cat}(s^{-1})$	431.9	418.8	401.4	401.4	436.3	436.3	479.9	479.9	379.6	567.2	523.6
$k_{cat}/s_{0.5}(s^{-1}\ mM^{-1})$	644.1	2626	2055	1348	1504	1008	2286	1778	319.8	404.6	350.9
ADP titration											
K_m (mM)	0.070 ± 0.015	NA[a]	NA	NA	NA	NA	NA	NA	0.147 ± 0.020	0.155 ± 0.026	0.146 ± 0.033
V_{max} (mM/min)	0.080 ± 0.005	NA	NA	NA	NA	NA	NA	NA	0.089 ± 0.004	0.067 ± 0.003	0.078 ± 0.005
$k_{cat}(s^{-1})$	349.0	NA	NA	NA	NA	NA	NA	NA	388.3	292.3	340.3
$k_{cat}/K_m(s^{-1}\ mM^{-1})$	4952	NA	NA	NA	NA	NA	NA	NA	2633	1876	2321

[a] NA, not applicable (the regulator had no significant effect on PykA kinetics compared with the control (no additive present)). The values of k_{cat} were calculated using $[E_t]$ = [PK monomer].

Table 2
Crystallographic data collection and refinement statistics of PykA
Values in parentheses are for the highest resolution shell.

PDB code	6QXL
Synchrotron/X-ray source	Diamond Light Source
Beamline	IO4-1
Data collection	
Wavelength (Å)	0.9159
Resolution range (Å)	405.44–2.43 (2.49–2.43)
Space group	$P3_1\ 2\ 1$
Unit cell	
a, *b*, *c*, (Å)	182.48, 182.48, 405.04
a, *b*, *g* (°)	90, 90, 120
Total reflections	4,318,494 (226,510)
Unique reflections	292,996 (21,477)
Multiplicity	14.7 (10.5)
Completeness (%)	100.0 (100.0)
Mean $I/\sigma(I)$	11.1 (1.1)
Resolution (Å) at mean $I/\sigma(I) > 2$	2.65 Å
Wilson *B*-factor	55.5
R_{merge}	0.143 (2.210)
R_{meas}	0.148 (2.324)
CC1/2	0.999 (0.642)
Refinement	
Resolution range (high resolution) (Å)	158.03–2.43 (2.49–2.43)
Reflections used in refinement	289,310 (21,209)
Reflections used for R_{free}	14,331 (1,071)
R_{work}	0.227 (0.298)
R_{free}	0.251 (0.315)
Number of molecules in the ASU	12
Number of non-hydrogen atoms	
Macromolecules	43,331
Ligands	306
Solvent	2,268
Protein residues	
RMS (bonds) (Å)	0.014
RMS (angles) (°)	1.64
Ramachandran favored (%)	96.98
Ramachandran allowed (%)	2.8
Ramachandran outliers (%)	0.23
Average *B*-factor	
Macromolecules	55.65
Ligands	62.51
Solvent	50.59

Kinetic analysis indicated that G6P is an activator of PykA, increasing the apparent catalytic efficiency ($k_{cat}/s_{0.5}$) of the enzyme around 3-fold (Table 1, Fig. 2, and Fig. S9). Inspection of the PykA structure revealed a molecule of G6P buried in each C-domain, far from the active site, indicating that G6P is an allosteric regulator (Fig. 3*B*). The structure of only one other bacterial PK with bound regulator has been solved, and that is the PykF family enzyme from *M. tuberculosis* (Mtb). A comparison of the allosteric binding site(s) observed in the Mtb enzyme reveals AMP bound in the same location as the G6P in *P. aeruginosa* PykA. The Mtb enzyme does bind G6P, but the ligand is located in an entirely different position in the allosteric cleft (PDB 5WSB) (Fig. 4*A*).

The G6P-binding pocket in PykA is comprised of two loops: a "phosphate loop" and a "ring loop." The phosphate loop (Cβ1-Cα2, residues 383–388) and partly the Cα2 helix (Thr^{389}) binds the phosphate group of the ligand, whereas the ring loop (Cβ4-Cβ5, residues 460–471) anchors the hexose ring moiety. Superposition of the G6P-binding site in PykA with the PykF apo-enzyme (PDB 1PKY) from *E. coli* reveals that in the presence of G6P, the ring loop of PykA is pulled tightly over the allosteric pocket (Fig. 4*B*), whereas the phosphate loop shares a similar disposition in both structures. The movement of the ring loop in the presence of G6P causes a shift and partial unwinding of the Cα4 helix in PykA.

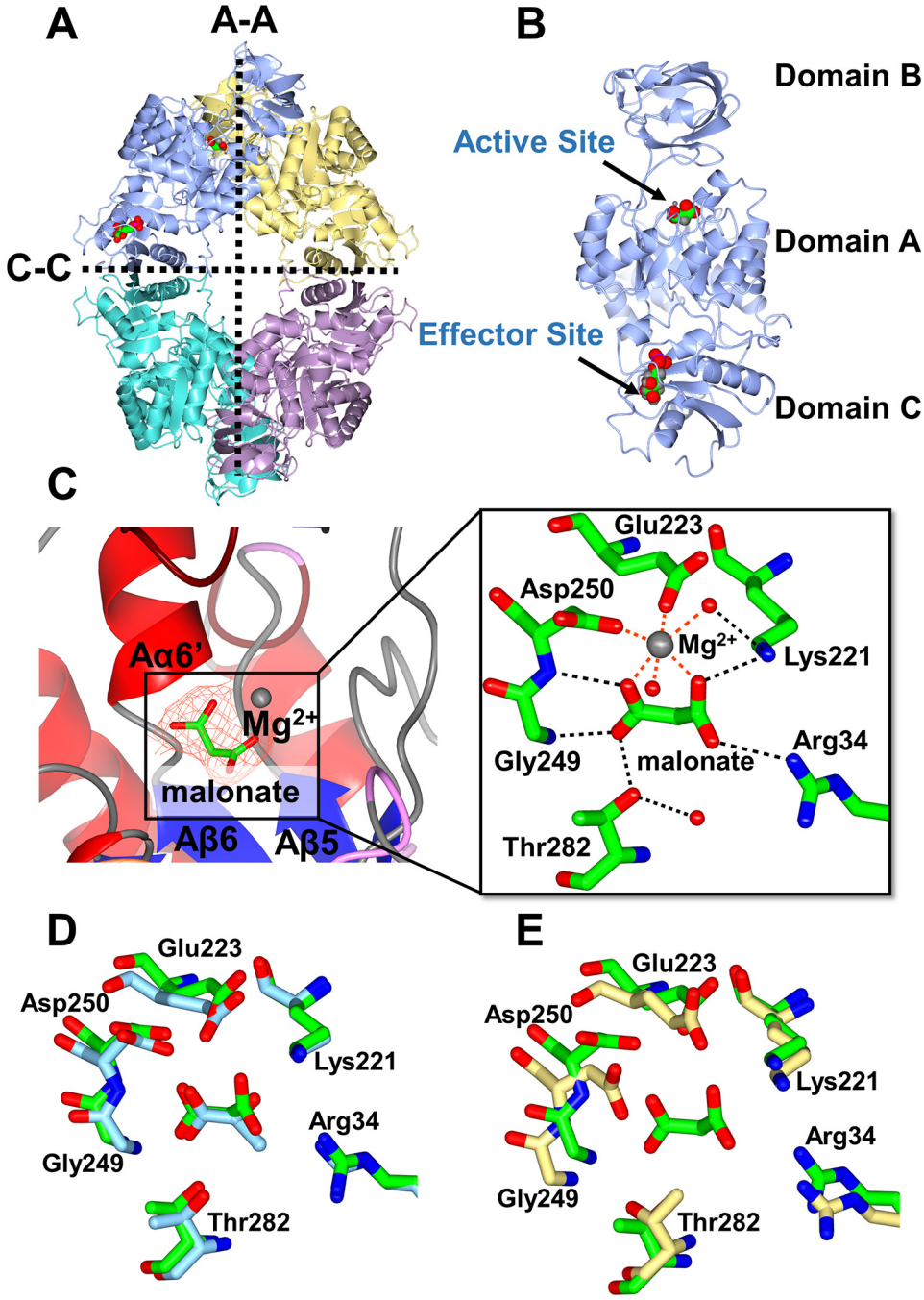

Figure 3. X-ray crystal structure of PykA. *A,* the PykA homotetramer. The A-A and C-C interfaces are shown. Substrate and G6P-binding sites are indicated in the *top left* protomer. *B,* domain organization of a PykA protomer showing malonate bound in the active site and G6P bound in the allosteric site. *C,* close-up of the PykA active site. The network of interactions involved in holding the malonate-Mg^{2+} (*orange mesh*, $F_o - F_c$ map contoured at 3σ) and water molecules are shown. *D,* superposition of the side chains involved in malonate binding in PykA (*green*) and pyruvate binding in rabbit muscle PK (PDB 1F3W, *light blue*). *E,* superposition of the side chains involved in malonate binding in *P. aeruginosa* PykA (*green*) with side chains present in the active site of *E. coli* PykF (PDB 1PKY, *yellow*).

The bound G6P interacts with the surrounding residues through a network of hydrogen bonds involving both the phosphate group and the sugar ring hydroxyls (Fig. 4*C*). In addition, occupation of the allosteric site also appears to promote secondary interactions between the phosphate loop and the ring loop of PykA; Ser^{386} and Thr^{389} on the phosphate loop form hydrogen bonds with Gln^{467} and Thr^{470} on the ring loop, respectively. Interestingly, Lys^{460} and Tyr^{464} on the ring loop also interact, tightening up closure of the binding pocket (Fig. 4*D*). This may be unique to the PK subclass represented by *P. aeruginosa* PykA, because its ring loop is less well-conserved than the ring loop in other PykA enzymes (Fig. S1). Furthermore, half of the residues that mediate the interaction between the phosphate and the ring loops are unique to *P. aeruginosa* PykA (Lys^{460}, Tyr^{464}, and Gln^{467}).

Comparison of the G6P-bound PykA structure with the *E. coli* apo-PykF structure (PDB 1PKY) revealed differences in the disposition of residues at the protomer interfaces. The

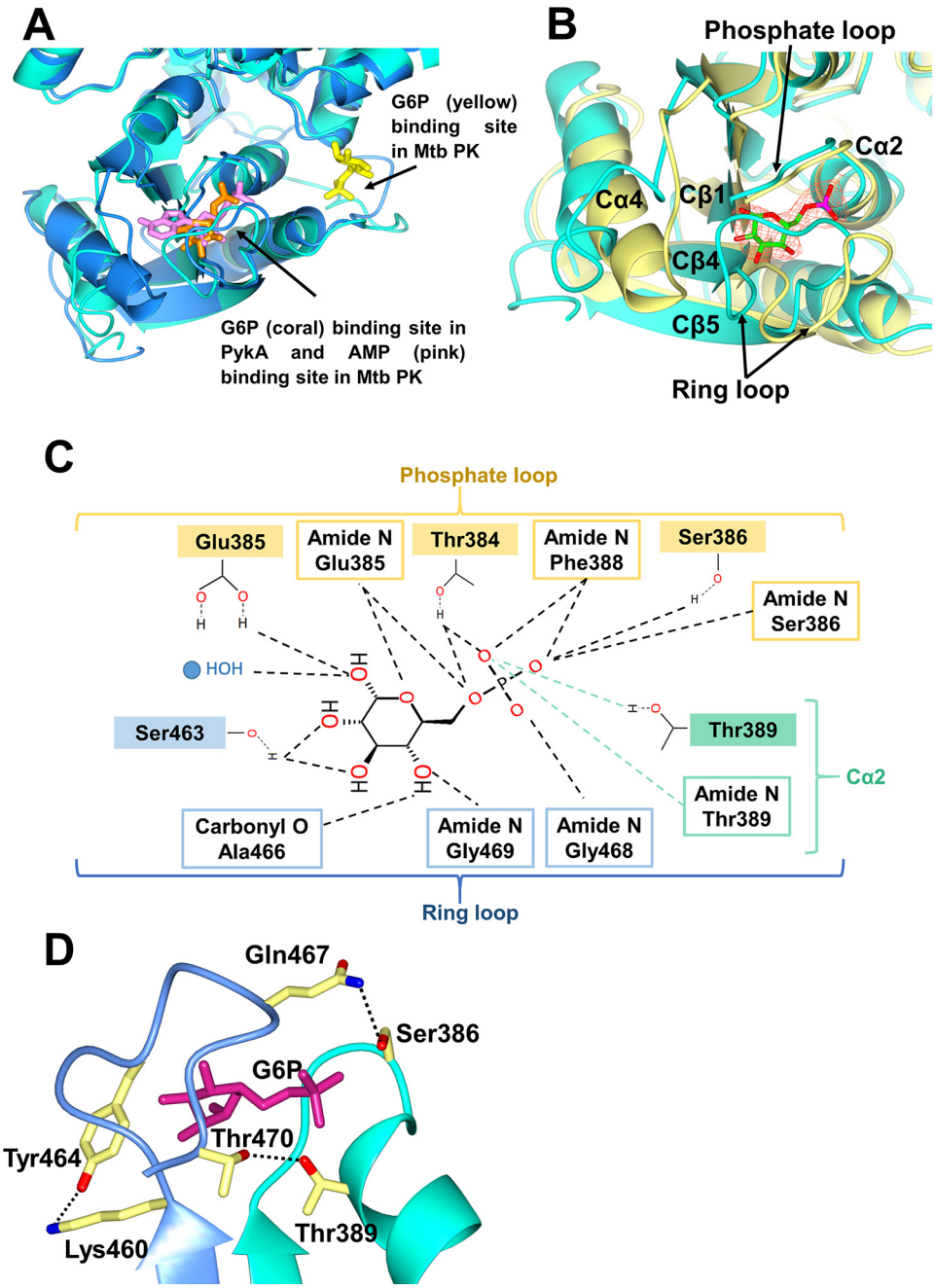

Figure 4. The G6P-binding site in PykA. *A,* superposition of the allosteric site in PykA from *P. aeruginosa* (*light green*) and PK from *M. tuberculosis* (PDB 5WSB, *blue*). The G6P in PykA is shown in *coral*, whereas the AMP and G6P in Mtb PK are shown in *pink* and *yellow*, respectively. *B,* superposition of the allosteric pocket in G6P-bound PykA (*light green*) and unbound PykF from *E. coli* (*yellow*). The G6P is shown surrounded by an electron density map (*orange mesh*, $F_o - F_c$ map contoured at 3σ). *C,* schematic of the interactions involved in binding G6P to PykA. *D,* interaction of the phosphate loop (*light green*) and ring loop (*blue*) in the G6P-binding site of PykA. The G6P is shown as *magenta sticks*.

PykA tetramer contains four inter-protomer interfaces, two of which are between adjacent A-domains (A-A interface) and two between adjacent C-domains (C-C interface) (Fig. 3*A*). The A-A interface (~1450 Å^2) is formed through pairing of Aα6, Aα6′, Aα7, Aα8, loop Aα6-Aα6′, loop Aα7-Aβ7, and loop Aα8-Cα1 from one protomer with the same secondary structural units (albeit, with inverted symmetry) on the second protomer (Fig. S11). By contrast, the apo-structure of PykF does not include Aα6′ or loop Aα8-Cα1 as parts of the interface and instead, there is an Aα7-Aα7 interaction that is absent in PykA (Fig. 5*A*). The A-A interface in PykA is very close to the active site, so structural changes at the interface affect the disposition of active site residues including Arg^{248}, Gly^{249}, Glu^{283}, Asp^{250}, and Thr^{282} (Fig. S12). Indeed, the main chain amide nitrogen of Gly^{249} is directly involved in binding the substrate analogue, whereas the amide carbonyl moiety of this residue forms a hydrogen bond with the side chain of Arg^{296} on helix Aα7 on the adjacent protomer (Fig. 5*C*). The A-A interface is stabilized by just two salt bridges (Fig. S13), which contrasts with the situation seen in *E. coli* apo-PykF, where most of the interactions at the A-A involve salt bridges.

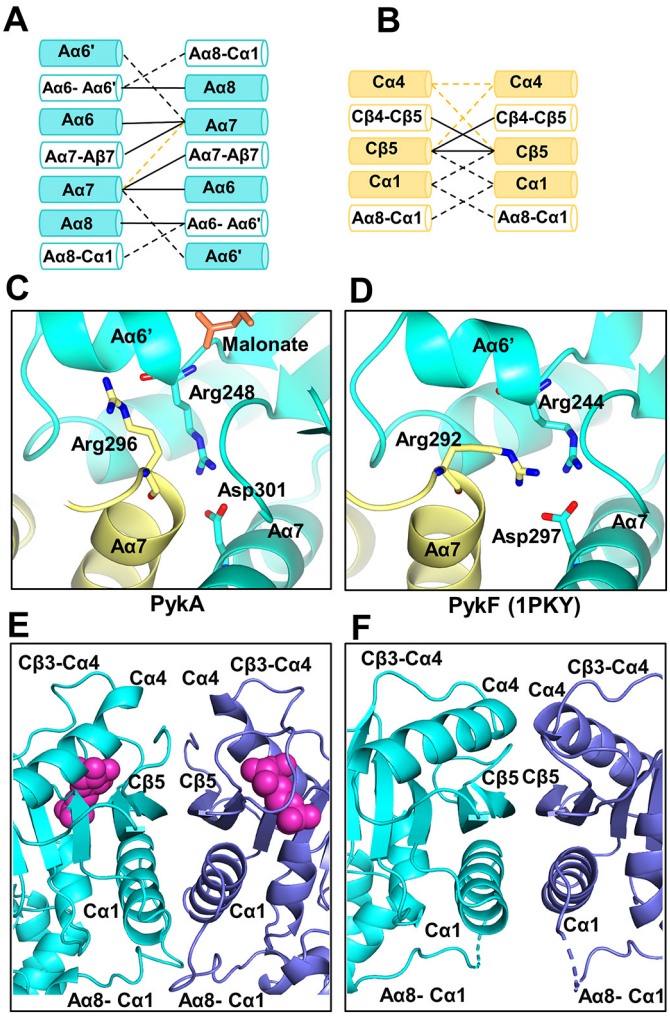

Figure 5. The inter-protomer interfaces in PykA. Comparison between (*A*) the A-A interface and (*B*) the C-C interface in PykA and *E. coli* PykF. Interactions present in both PykA and PykF are shown as *solid black lines*. Interactions unique to PykA only are shown as *black dashed lines*. Interactions unique to PykF only are shown as *yellow dashed lines*. *C,* close-up view of the A-A interface in PykA showing Arg^{296} oriented toward the active site. *D,* close-up view of the A-A interface in *E. coli* PykF showing Arg^{292} (equivalent to Arg^{296} in PykA) oriented away from the active site. *E,* the C-C interface in PykA. G6P is depicted as *large magenta spheres*. *F,* the C-C interface in *E. coli* PykF.

Comparison of G6P-bound PykA with apo-PykF (PDB 1PKY) also reveals major differences at the C-C interface (Fig. 5*B*). The C-C interface in PykF is comprised of Cα4, Cβ5, and the ring loop between Cβ4 and Cβ5. By contrast, the C-C interface in PykA is comprised of Cβ5, the ring loop, Cα1, and the long, flexible loop between Aα8-Cα1. Essentially, the bound G6P in PykA displaces the ring loop and Cα4, resulting in an outward movement of Cα1. This drags the Aα8-Cα1 loop region closer toward the C-C interface (Fig. 5, *E* and *F*). This movement of the Aα8-Cα1 loop could, in turn, communicate the conformational change from the G6P-binding site to the A-A interface and the active site, providing a plausible mechanism by which the allosteric regulator elicits its effect.

Discussion

Consistent with its role as the major PK isozyme in *P. aeruginosa*, a *pykA* mutant was defective in growth on glucose and glycerol. These data raise the question of why *P. aeruginosa* encodes two distinct PK isozymes? This is intriguing, especially given that the gene encoding one of the isozymes (*pykF*) appeared to show negligible expression under any of the growth conditions tested. One likely solution is that *pykF* appears to be part of a larger cluster of genes (PA1498–PA1502) that may be involved in the catabolism of compounds such as ethylene glycol (20). Therefore, although artificially expressed *pykF* is capable of rescuing the growth defect associated with the *pykA* mutant (Fig. 1), its expression is likely to be induced only under very select conditions.

P. aeruginosa lacks phosphofructokinase (encoded by *pfk*) and is therefore incapable of carrying out the EMP pathway of glycolysis (13). Instead, and in common with around 13% of species for which a genome sequence is available, it is exclusively reliant on the EDP for glucose oxidation (21). In this pathway, pyruvate kinase is the major regulatory enzyme. PykA activity was activated primarily by G6P, F6P, G3P, and by intermediates of the reductive PPP. In many organisms, the upper arm of the reductive PPP is "fed" by the conversion of 6-phosphogluconate into ribulose 5-phosphate; a reaction catalyzed by 6-phosphogluconate dehydrogenase (*gnd*) (22–24). However, and like many other bacteria that exclusively utilize the EDP, *P. aeruginosa* does not encode a homologue of *gnd* (13, 25). As a consequence, carbon can only flow into the PPP from G3P or from gluconeogenesis-derived F6P (Fig. 6) (26). Not surprisingly, given the lack of redundancy in input pathways, many of the PPP-encoding genes are essential in *P. aeruginosa* (26). It is therefore logical that *P. aeruginosa* has evolved to coordinate glucose oxidation with the supply of biosynthetic precursors by titrating both gluconeogenic and PPP intermediates. These two anabolic pathways are tightly inter-twined; as shown in Fig. 6, EDP-derived G3P, and F6P derived from gluconeogenesis also play a central role in the cyclical series of sugar phosphate interconversions that comprise the reductive PPP. High levels of these, and other key PPP intermediates (R5P, X5P, and RL5P) are presumably physiological indicators that biosynthetic precursors are abundant (27), and that carbon flux can be redirected toward energy production via PykA activation. Similarly, high levels of G6P indicate sufficiency of either glucose supply or of gluconeogenic flux, so it makes good metabolic sense that this too should feed forward to stimulate PykA, and hence, carbon catabolism.

The only other bacterial PK structure containing bound regulatory ligands is the PK from *M. tuberculosis* (28). That work revealed that AMP binds in the heart of the C domain (Fig. 4*A*), and that G6P binds at the interface between the A and C domains. However, *P. aeruginosa* PykA was insensitive to AMP, and G6P was found to be bound to the same site as that occupied by AMP in the Mtb structure. This indicates that although the allosteric binding pocket is conserved as a cavity in PykA, there is considerable evolutionary plasticity in regulator binding. That different enzymes from the same family (albeit, from different species) have evolved to bind the same allosteric regulator (G6P) in different sites is remarkable, especially from the perspective of allosteric transitions. Moreover, and given the radically different structures of ring-sugar phosphates such as G6P and F6P compared with "configurationally locked"

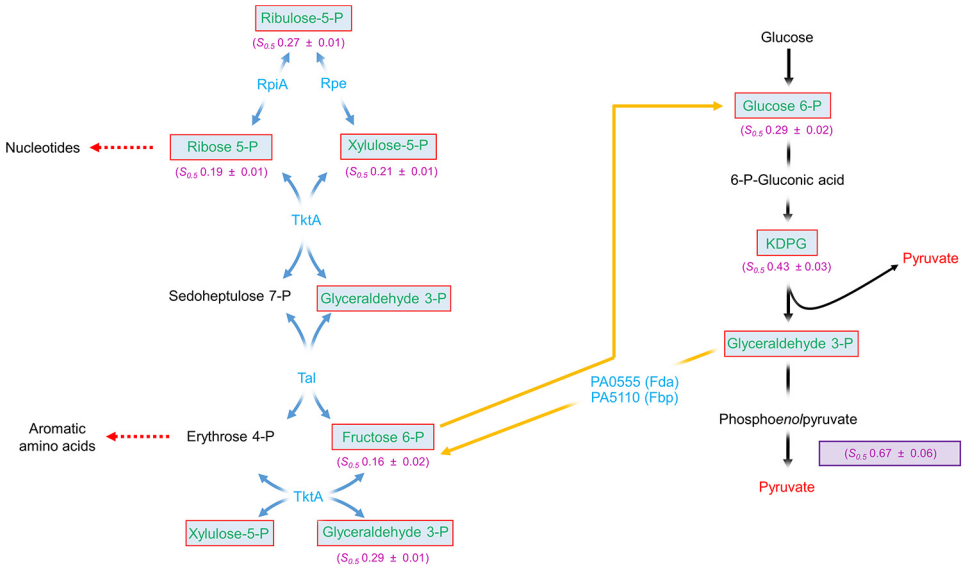

Figure 6. PykA is primarily regulated by PPP metabolites. Pathways of glucose metabolism in *P. aeruginosa* are indicated by *black* (EDP), *blue* (PPP), and *yellow* (EMP) *arrows*, respectively. Identified PykA regulators are *boxed* and shown in *green* with the respective $s_{0.5}$ indicated *below* each regulator. Fructose 6-phosphate and glyceraldehyde 3-phosphate are depicted as part of the PPP to emphasize the importance they play in this series of sugar interconversions. The $s_{0.5}$ of PykA without regulators is shown in a *violet box*. *RpiA*, ribose 5-phosphate isomerase; *Rpe*, ribulose phosphate 3-epimerase; *TktA*, transketolase; *Tal*, transaldolase; *Fda*, fructose 1,6-bisphosphate aldolase; *Fbp*, fructose 1,6-bisphosphatase.

straight-chain forms such as RL5P and X5P, this suggests that the latter may well bind PykA at other, yet to be characterized sites.

Unfortunately, we were unable to obtain crystals of apo-PykA that diffracted beyond about 4 Å. We therefore based our structural comparisons on the PykF apoenzyme from *E. coli*, which does not contain bound substrate or regulatory ligands. In the PykF structure, the allosteric pocket is open, and is uncapped by the ring loop (29). This unbound configuration allows the Cα4 helices to form prominent interactions across the C-C interface. However, when the allosteric site becomes occupied by G6P, the ring loop is pulled down toward the ligand. This partially displaces Cα4 and firmly closes the allosteric pocket through interactions with both the ligand and the phosphate loop. The new configuration of the allosteric site seems to loosen up the interactions from Cα4, concomitantly recruiting other structures to the interface, most notably Cα1 and the Aα8-Cα1 loop (Fig. 5). Thus, in PykA, the Aα8-Cα1 loop contacts two protomers simultaneously via the A-A interface and the C-C interface. Given the proximity of the A-A interface with the active site, this suggests a likely mechanism by which G6P binding may influence catalysis. Fig. 7 illustrates this proposed mechanism. G6P binding to the allosteric pocket leads to movement of the ring loop, which displaces Cα4 and allows outward movement of Cα1. This, in turn, leads to a restructuring of the Aα8-Cα1 loop, which directly or indirectly affects the A-A interface, especially Aα6′ (which forms part of the active site). This proposed mechanism contrasts with the rigid-body rock-shape-lock mechanism proposed for Mtb PK (28).

Materials and methods

For primers and bacterial strains, see Table S1.

Construction of mutants

The *pykA* and *pykF* mutants used were from the Washington Mutant Library (identities PW8308 (*pykA*-B04::ISlacZ/hah, which carries a Tn insertion at position 903/1452) and PW3705 (*pykF*-C02::ISphoA/hah, which carries a Tn insertion at position 213/1434), respectively). The insertion site of the transposon in each mutant was confirmed by PCR using the primers recommended by the library curators. To generate the *pykA pykF* double mutant, we first had to remove the Tet^R marker from the *pykA* mutant. This was done by introducing plasmid pFLP2-cre into the *pykA* mutant by electroporation (to enable site-specific cre-mediated excision of the transposon) followed by plasmid curing on LBA plates containing 5% sucrose (pFLP2-cre carries *sacB* as a counter-selectable marker). Site-specific excision of the Tet^R marker leaves behind a 63-codon scar within the target gene, and this was confirmed using PCR (Fig. S3). The Tet^S *pykA* mutant was then used as a recipient for the Tet^R marker from a *pykF* donor, introduced by generalized transduction with ϕPA3 as a vehicle (30). The *pykA pykF* double mutant was confirmed using (i) PCR to demonstrate the presence of the 63 codon scar in the *pykA* ORF (Fig. S3), (ii) the absence of a PCR-amplifiable *pykF* fragment in the transductants (Fig. S4), and (iii) the Tet^R phenotype of the transductants.

Construction of complementing plasmids

To complement the *pykA* mutant, a region encompassing the entire *pykA* ORF and 500 bp upstream of this were PCR-amplified using primers *pykA*-pLP170-FD and *pykA*-pET19m-RV. The amplified DNA fragment was digested with EcoRI and BamHI and introduced into similarly digested pUCP20, yielding p*pykA*$^+$. To complement the *pykF* mutant, we used a different strategy. The *pykF* ORF is predicted to form an operon with an adjacent glycerate kinase-encoding gene, PA1499. Therefore, we PCR amplified the entire region spanning from

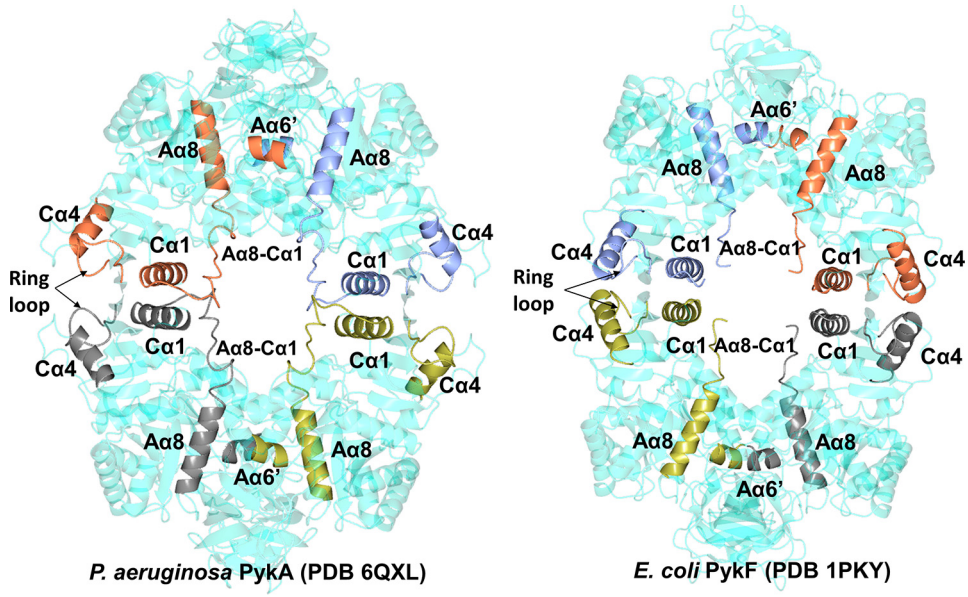

Figure 7. Spatial disposition of key secondary structural elements in *P. aeruginosa* PykA and *E. coli* PykF. Note how the movement of the ring loop in PykA leads to disruption of the Cα4-Cα4 interaction and concomitant outward movement of Cα1. This, in turn, tugs on the Aα8-Cα1 loop, engaging it with the C-C interface. The resulting movement of Aα8 directly or indirectly affects the A-A interface by forming new interactions with Aα6-Aα6′. Given that Aα6′ forms part of the active site, this set of interactions provides a plausible mechanism by which G6P binding to the allosteric pocket in the structure can lead to altered catalysis.

upstream of PA1499 to the 3′ end of *pykF* (using primers PA1499-pLP170-FD and *pykF*-pET19m-RV primers). The amplified DNA fragment was digested with EcoRI and HindIII and introduced into similarly digested pUCP20, yielding p*pykF*$^{+}$.

Bacterial growth

The indicated strains/mutants were grown in LB overnight and washed twice in PBS. Cultures were inoculated to an initial A_{600} of 0.05 in 50 ml of minimal media containing the indicated carbon sources and/or antibiotics. The cultures were grown at 37 °C with vigorous aeration. Samples were taken every hour for optical density measurement. Each growth curve was carried out in triplicate.

Enzyme assays

Cultures were grown in 50 ml of minimal media containing the indicated carbon sources and/or antibiotics. The cultures were grown at 37 °C with vigorous aeration. After the indicated period of growth, the cells were harvested by centrifugation (3220 × *g*, 15 min, 4 °C) and resuspended in lysis buffer (50 mM Tris-HCl, 0.1 M NaCl, pH 7.5) containing a protease inhibitor mixture tablet (Roche, 1 tablet per 50 ml of buffer). The cells were lysed by sonication on ice and the lysates were clarified by centrifugation. Protein was determined using the Bradford assay. PK activity was measured using a lactate dehydrogenase (LDH)-coupled assay. The reaction mixtures contained 50 mM Tris-HCl (pH 7.5), 10 mM $MgCl_2$, 10 units of rabbit muscle LDH, 0.2 mM NADH, 5 mM PEP, and 2 mM ADP. Reactions were initiated by the addition of an equal volume of cell lysate (normalized for protein concentration) and allowed to proceed at 37 °C. NADH consumption was monitored at 340 nm. Each measurement was carried out in triplicate.

Kinetics of purified PykA

Pyruvate kinase activity was measured at 37 °C in 1-ml reactions containing 50 mM Tris-HCl, 10 mM $MgCl_2$, 10 units of rabbit muscle LDH, 0.2 mM NADH (pH 7.5). For the PEP titrations, [ADP] was kept constant at 2 mM. For the ADP titrations, [PEP] was kept constant at 5 mM. Reactions were initiated by addition of purified PykA to a final concentration of 0.2 μg/ml. Reaction progress was monitored at 340 nm. Regulator screens were carried out using 1 mM final concentration of the indicated regulator candidates and a fixed concentration of either 2 mM ADP and 0.3 mM PEP (when screening for activators), or 2 mM ADP and 2 mM PEP (when screening for inhibitors). The effect of the hits identified this way on the detailed kinetics were re-measured with 1 mM of each potential regulator and variable concentrations of PEP and ADP, as above. The only exception to this was that F6P, R5P, and X5P were added at 0.2, 0.15, and 0.5 mM final concentrations, respectively, in all experiments. GraphPad Prism 7 was used to analyze the data and to extract the kinetic constants. All experiments were carried out in triplicate.

Western blotting

Anti-PykA and anti-PykF antibodies were raised against purified PykA and PykF proteins, respectively (Biogenes.De). The PykA and PykF antisera were pre-absorbed onto an acetone extract of whole lysate protein from a *pykA* mutant or from a *pykF* mutant, respectively. The primary anti-PykA and anti-PykF antibodies were used at 1:2,000 and 1:3,000 dilution, respectively. Horseradish peroxidase-conjugated goat anti-rabbit (1:10,000) was used as a secondary antibody. The isocitrate dehydrogenase isozyme, ICD, was used as a loading control. Antibodies raised against ICD has been described previously (31).

Cloning, expression, and purification of PykA and PykF

The ORFs encoding PykA (PA4329) and PykF (PA1498) were PCR-amplified from *P. aeruginosa* genomic DNA using primers *pykA*-pET19m-FD and *pykA*-pET19m-RV (for *pykA* amplification) and *pykF*-pET19m-FD and *pykF*-pET19m-RV (for *pykF* amplification). The amplified ORFs were cloned into pET-19m, generating pET-19m (*pykA*) and pET-19m (*pykF*), respectively. Expression from pET-19m yields a tobacco etch virus protease-cleavable N terminally His_6-tagged protein product. For protein expression, *E. coli* BL21 (DE3) containing pET-19m (*pykA*) or pET-19m (*pykF*), as appropriate, was grown in 1 liter of LB containing 50 μg/ml of carbenicillin and 34 μg/ml of chloramphenicol at 37 °C until the A_{600} reached 0.5. The temperature was then decreased to 20 °C and protein expression was induced by adding isopropyl β-D-thiogalactopyranoside to a final concentration of 1 mM. Following overnight growth, the cells were harvested by centrifugation (4,000 × *g*, 30 min, 4 °C) and re-suspended in 50 ml of ice-cold lysis buffer (50 mM Tris-HCl, 200 mM NaCl, 10% (v/v) glycerol, 10 mM imidazole (pH 8.0)) containing a dissolved EDTA-free protease inhibitor mixture tablet (Roche). The resuspended cells were lysed by sonication on ice and the sample was then clarified by sedimentation (10,000 × *g*, 30 min, 4 °C). The clear supernatant was loaded onto an nickel-nitrilotriacetic acid column that had been previously pre-equilibrated with lysis buffer. The column was washed overnight with lysis buffer. The bound protein was eluted in 50 mM Tris-HCl, 200 mM NaCl, 10% (v/v) glycerol, 250 mM imidazole (pH 8.0). The eluted protein was mixed with His_6-tagged tobacco etch virus protease (1 mg/20 mg of target protein) and loaded into a dialysis bag (10,000 MWCO). The sample was dialyzed overnight against 20 mM Tris-HCl, 100 mM NaCl, 5% (v/v) glycerol, 1 mM DTT, 0.1 mM EDTA (pH 7.5). After dialysis, the protein was transferred into a Falcon tube and incubated end-over-end for 2 h at 4 °C with a slurry of nickel-nitrilotriacetic acid that had been previously pre-equilibrated in dialysis buffer. Unbound protein was concentrated by ultrafiltration (Vivaspin column, 30,000 MWCO) then aliquoted and flash frozen in liquid nitrogen. The protein concentration was determined by spectrophotometry using a calculated molar extinction coefficient of 24,410 M^{-1} cm^{-1} for PykA and 25,440 $M^{-1}cm^{-1}$ for PykF.

Analytical ultracentrifugation

Purified PykA was dialyzed against 20 mM Tris-HCl, 100 mM NaCl, and 0.1 mM EDTA (pH 7.5) for glycerol removal. The centerpieces of the Epon double-sector of a Beckman Optima XL-I (AN-60 Ti rotor) were filled with 400 μl of purified protein or blank buffer. The sample was sedimented at 29,160 × *g*, for 24 h at 20 °C. Absorbance data (280 nm) were acquired every 2 min with interference scans collected every minute. Data analysis and the calculations of buffer viscosity, protein partial specific volumes, and frictional rations were performed using SEDFIT and SEDNTERP (32, 33).

Amino acid sequence analysis

Amino acid sequences were extracted from UniProt in FASTA format, aligned by Clustal Omega (34, 35), and displayed by ESPript (36).

Crystallization of PykA

PykA was crystallized using the sitting drop vapor diffusion method. PykA (22 mg/ml in 20 mM Tris-HCl, 100 mM NaCl, 5% (v/v) glycerol, 1 mM DTT, 0.1 mM EDTA, 20 mM $MgCl_2$, 2 mM G6P, 2 mM PEP (pH 7.5)) was mixed 1:1 with the reservoir buffer (200 nl each), which contained 20% (w/v) PEG3350, 0.1 M BIS-TRIS propane, and 0.2 M disodium malonate (pH 7.5). Crystals grew within 1 week. The crystals were mounted on nylon loops and cryoprotected in mother liquor supplemented with 40% (v/v) glycerol before being flash frozen in liquid N_2.

X-ray diffraction and structure refinement

Diffraction data were collected at the Diamond Light Source (Didcot, UK) on beamline IO4 (MX14043-47). The PykA structure was obtained from molecular replacement with Phaser (37) using the pyruvate kinase of *Trypanosoma brucei* (PDB 4HYV) as a structural template. Coot (38) was used for model building, and refinement was performed by BUSTER (39). Table 2 shows the data collection and refinement statistics. Structural coordinates were deposited in the PDB with accession code PDB 6QXL. PDBePISA (40) was used for analysis of the tetramer and ligand interfaces. Figures were generated using CCP4mg and PyMOL (41, 42).

Author contributions—Y. A. and M. W. conceptualization; Y. A., P. B., J. G., X. C., T. R., and M. W. formal analysis; Y. A., T. R., and M. W. supervision; Y. A. and M. W. funding acquisition; Y. A., P. B., J. G., X. C., and T. R. investigation; Y. A., P. B., and M. W. methodology; Y. A., P. B., and M. W. writing-original draft; Y. A. and M. W. project administration; Y. A., P. B., J. G., X. C., T. R., and M. W. writing-review and editing; P. B. and J. G. resources.

References

1. Kayne, F. J. (1973) 11 Pyruvate kinase. *Enzymes* **8,** 353–382 CrossRef
2. Al Zaid Siddiquee, K., Arauzo-Bravo, M. J., and Shimizu, K. (2004) Metabolic flux analysis of *pykF* gene knockout *Escherichia coli* based on ^{13}C-labeling experiments together with measurements of enzyme activities and intracellular metabolite concentrations. *Appl. Microbiol. Biotechnol.* **63,** 407–417 CrossRef Medline
3. Sawada, K., Zen-in, S., Wada, M., and Yokota, A. (2010) Metabolic changes in a pyruvate kinase gene deletion mutant of *Corynebacterium glutamicum* ATCC 13032. *Metab. Eng.* **12,** 401–407 CrossRef Medline
4. Bücker, R., Heroven, A. K., Becker, J., Dersch, P., and Wittmann, C. (2014) The pyruvate-tricarboxylic acid cycle node: a focal point of virulence control in the enteric pathogen *Yersinia pseudotuberculosis*. *J. Biol. Chem.* **289,** 30114–30132 CrossRef Medline
5. Ponce, E., Flores, N., Martinez, A., Valle, F., and Bolívar, F. (1995) Cloning of the two pyruvate kinase isoenzyme structural genes from *Escherichia coli*: the relative roles of these enzymes in pyruvate biosynthesis. *J. Bacteriol.* **177,** 5719–5722 CrossRef Medline
6. Garcia-Olalla, C., and Garrido-Pertierra, A. (1987) Purification and kinetic properties of pyruvate kinase isoenzymes of *Salmonella typhimurium*. *Biochem. J.* **241,** 573–581 CrossRef Medline
7. Hofmann, J., Heider, C., Li, W., Krausze, J., Roessle, M., and Wilharm, G. (2013) Recombinant production of *Yersinia enterocolitica* pyruvate kinase isoenzymes PykA and PykF. *Protein Expr. Purif.* **88,** 243–247 CrossRef Medline
8. Waygood, E. B., Mort, J. S., and Sanwal, B. D. (1976) The control of pyruvate kinase of *Escherichia coli*: binding of substrate and allosteric effectors to the enzyme activated by fructose 1,6-bisphosphate. *Biochemistry* **15,** 277–282 CrossRef Medline

9. Waygood, E. B., Rayman, M. K., and Sanwal, B. D. (1975) The control of pyruvate kinases of *Escherichia coli*: II. effectors and regulatory properties of the enzyme activated by ribose 5-phosphate. *Can. J. Biochem.* **53,** 444–454 CrossRef Medline
10. Martínez-Solano, L., Macia, M. D., Fajardo, A., Oliver, A., and Martinez, J. L. (2008) Chronic *Pseudomonas aeruginosa* infection in chronic obstructive pulmonary disease. *Clin. Infect. Dis.* **47,** 1526–1533 CrossRef Medline
11. Mittal, R., Aggarwal, S., Sharma, S., Chhibber, S., and Harjai, K. (2009) Urinary tract infections caused by *Pseudomonas aeruginosa*: a minireview. *J. Infect. Public Health* **2,** 101–111 CrossRef Medline
12. Williamson, K. S., Richards, L. A., Perez-Osorio, A. C., Pitts, B., McInnerney, K., Stewart, P. S., and Franklin, M. J. (2012) Heterogeneity in *Pseudomonas aeruginosa* biofilms includes expression of ribosome hibernation factors in the antibiotic-tolerant subpopulation and hypoxia-induced stress response in the metabolically active population. *J. Bacteriol.* **194,** 2062–2073 CrossRef Medline
13. Lessie, T. G., and Phibbs, P. V. (1984) Alternative pathways of carbohydrate utilization in *Pseudomonads*. *Annu. Rev. Microbiol.* **38,** 359–388 CrossRef Medline
14. Kersters, K., and De Ley, J. (1968) The occurrence of the Entner-Doudoroff pathway in bacteria. *Antonie Van Leeuwenhoek* **34,** 393–408 CrossRef Medline
15. Nikel, P. I., Chavarría, M., Fuhrer, T., Sauer, U., and de Lorenzo, V. (2015) *Pseudomonas putida* KT2440 strain metabolizes glucose through a cycle formed by enzymes of the Entner-Doudoroff, Embden-Meyerhof-Parnas, and pentose phosphate pathways *J. Biol. Chem.* **290,** 25920–25932 CrossRef Medline
16. Kachmar, J. F., and Boyer, P. D. (1953) Kinetic analysis of enzyme reactions: II. the potassium activation and calcium inhibition of pyruvic phosphoferase. *J. Biol. Chem.* **200,** 669–682 Medline
17. Larsen, T. M., Benning, M. M., Wesenberg, G. E., Rayment, I., and Reed, G. H. (1997) Ligand-induced domain movement in pyruvate kinase: structure of the enzyme from rabbit muscle with Mg^{2+}, K^+, and L-phospholactate at 2.7 Å resolution *Arch. Biochem. Biophys.* **345,** 199–206 CrossRef
18. Oria-Hernández, J., Cabrera, N., Pérez-Montfort, R., and Ramírez-Silva, L. (2005) Pyruvate kinase revisited: the activating effect of K^+. *J. Biol. Chem.* **280,** 37924–37929 CrossRef Medline
19. Laughlin, L. T., and Reed, G. H. (1997) The monovalent cation requirement of rabbit muscle pyruvate kinase is eliminated by substitution of lysine for glutamate 117. *Arch. Biochem. Biophys.* **348,** 262–267 CrossRef Medline
20. Franden, M. A., Jayakody, L. N., Li, W.-J., Wagner, N. J., Cleveland, N. S., Michener, W. E., Hauer, B., Blank, L. M., Wierckx, N., Klebensberger, J., and Beckham, G. T. (2018) Engineering *Pseudomonas putida* KT2440 for efficient ethylene glycol utilization. *Metab. Eng.* **48,** 197–207 CrossRef Medline
21. Flamholz, A., Noor, E., Bar-Even, A., Liebermeister, W., and Milo, R. (2013) Glycolytic strategy as a tradeoff between energy yield and protein cost. *Proc. Natl. Acad. Sci. U.S.A.* **110,** 10039–10044 CrossRef Medline
22. Scott, D. B. M., and Cohen, S. S. (1953) The oxidative pathway of carbohydrate metabolism in *Escherichia coli*: 1. the isolation and properties of glucose 6-phosphate dehydrogenase and 6-phosphogluconate dehydrogenase. *Biochem. J.* **55,** 23–33 CrossRef Medline
23. Scott, D. B., and Cohen, S. S. (1957) The oxidative pathway of carbohydrate metabolism in *Escherichia coli*: V. isolation and identification of ribulose phosphate produced from 6-phosphogluconate by the dehydrogenase of E. coli. *Biochem. J.* **65,** 686–689 CrossRef Medline
24. McNair Scott, D. B. (1956) The oxidative pathway of carbohydrate metabolism in *Escherichia coli*: III. glucose 6-phosphate dehydrogenase and 6-phosphogluconate dehydrogenase in cells grown under different conditions. *Biochem. J.* **63,** 587–593 CrossRef Medline
25. Mithani, A., Hein, J., and Preston, G. M. (2011) Comparative analysis of metabolic networks provides insight into the evolution of plant pathogenic and nonpathogenic lifestyles in *Pseudomonas*. *Mol. Biol. Evol.* **28,** 483–499 CrossRef Medline
26. Lee, S. A., Gallagher, L. A., Thongdee, M., Staudinger, B. J., Lippman, S., Singh, P. K., and Manoil, C. (2015) General and condition-specific essential functions of *Pseudomonas aeruginosa*. *Proc. Natl. Acad. Sci. U.S.A.* **112,** 5189–5194 CrossRef Medline
27. Stincone, A., Prigione, A., Cramer, T., Wamelink, M. M., Campbell, K., Cheung, E., Olin-Sandoval, V., Grüning, N.-M., Krüger, A., Tauqeer Alam, M., Keller, M. A., Breitenbach, M., Brindle, K. M., Rabinowitz, J. D., and Ralser, M. (2015) The return of metabolism: biochemistry and physiology of the pentose phosphate pathway. *Biol. Rev. Camb. Philos. Soc.* **90,** 927–963 CrossRef Medline
28. Zhong, W., Cui, L., Goh, B. C., Cai, Q., Ho, P., Chionh, Y. H., Yuan, M., Sahili, A. E., Fothergill-Gilmore, L. A., Walkinshaw, M. D., Lescar, J., and Dedon, P. C. (2017) Allosteric pyruvate kinase-based "logic gate" synergistically senses energy and sugar levels in *Mycobacterium tuberculosis*. *Nat. Commun.* **8,** 1986 CrossRef Medline
29. Mattevi, A., Valentini, G., Rizzi, M., Speranza, M. L., Bolognesi, M., and Coda, A. (1995) Crystal structure of *Escherichia coli* pyruvate kinase type I: molecular basis of the allosteric transition. *Structure* **3,** 729–741 CrossRef Medline
30. Monson, R., Foulds, I., Foweraker, J., Welch, M., and Salmond, G. P. (2011) The *Pseudomonas aeruginosa* generalized transducing phage PA3 is a new member of the KZ-like group of "jumbo" phages, and infects model laboratory strains and clinical isolates from cystic fibrosis patients. *Microbiology* **157,** 859–867 CrossRef Medline
31. Crousilles, A., Dolan, S. K., Brear, P., Chirgadze, D. Y., and Welch, M. (2018) Gluconeogenic precursor availability regulates flux through the glyoxylate shunt in *Pseudomonas aeruginosa*. *J. Biol. Chem.* **293,** 14260–14269 CrossRef Medline
32. Schuck, P. (2000) Size-distribution analysis of macromolecules by sedimentation velocity ultracentrifugation and Lamm equation modeling. *Biophys. J.* **78,** 1606–1619 CrossRef Medline
33. Hayes, D., Laue, T., and Philo, J. (1995) *Program Sednterp: Sedimentation Interpretation Program*. Alliance Protein Laboratories, Thousand Oaks, CA
34. Goujon, M., McWilliam, H., Li, W., Valentin, F., Squizzato, S., Paern, J., and Lopez, R. (2010) A new bioinformatics analysis tools framework at EMBL-EBI. *Nucleic Acids Res.* **38,** W695–W699 CrossRef Medline
35. Sievers, F., Wilm, A., Dineen, D., Gibson, T. J., Karplus, K., Li, W., Lopez, R., McWilliam, H., Remmert, M., Söding, J., Thompson, J. D., and Higgins, D. G. (2011) Fast, scalable generation of high-quality protein multiple sequence alignments using Clustal Omega. *Mol. Syst. Biol.* **7,** 539–539 Medline
36. Robert, X., and Gouet, P. (2014) Deciphering key features in protein structures with the new ENDscript server. *Nucleic Acids Res.* **42,** W320–W324 CrossRef Medline
37. McCoy, A. J., Grosse-Kunstleve, R. W., Adams, P. D., Winn, M. D., Storoni, L. C., and Read, R. J. (2007) Phaser crystallographic software. *J. Appl. Crystallogr.* **40,** 658–674 CrossRef Medline
38. Emsley, P., Lohkamp, B., Scott, W. G., and Cowtan, K. (2010) Features and development of Coot. *Acta Crystallogr. D Biol. Crystallogr.* **66,** 486–501 CrossRef Medline
39. Blanc, E., Roversi, P., Vonrhein, C., Flensburg, C., Lea, S. M., and Bricogne, G. (2004) Refinement of severely incomplete structures with maximum likelihood in *BUSTER–TNT*. *Acta Crystallogr. D Biol. Crystallogr.* **60,** 2210–2221 CrossRef
40. Krissinel, E., and Henrick, K. (2007) Inference of macromolecular assemblies from crystalline state. *J. Mol. Biol.* **372,** 774–797 CrossRef Medline
41. McNicholas, S., Potterton, E., Wilson, K. S., and Noble, M. E. M. (2011) Presenting your structures: the CCP4mg molecular-graphics software. *Acta Crystallogr. D Biol. Crystallogr.* **67,** 386–394 CrossRef
42. DeLano, W. L. (2012) *The PyMOL Molecular Graphics System, Version 2.0*, Schrödinger, LLC, New York